Theor Chem Acc (2006) 115: 212–220
DOI 10.1007/s00214-005-0007-y

REGULAR ARTICLE

J. Grant Hill · Peter B. Karadakov · David L. Cooper

A spin-coupled study of the Claisen rearrangement of allyl vinyl ether

Received: 18 October 2004 / Accepted: 5 May 2005 / Published online: 15 October 2005

Abstract The spin-coupled (SC) form of modern valence bond (VB) theory is utilised to examine the electronic structure of the transition state (TS) and the electronic reaction mechanism of the Claisen rearrangement of allyl vinyl ether. The differences between the spin-coupling patterns and orbital overlap integrals at the optimised TS geometries obtained using B3LYP/6-31G*, MP2/6-31G* and MP4(SDQ)/6-31G* wavefunctions are minimal, and the SC picture suggests that the TS is non-aromatic. SC calculations along the intrinsic reaction coordinates computed at these three levels of theory also produce near identical results. The SC wavefunctions at different stages of the reaction provide easily interpretable orbital diagrams which, in combination with the changes in the orbital overlap integrals, indicate an electronic reaction mechanism involving concerted, though not entirely synchronous, bond breaking and bond formation processes. The evolution of the active space spin-coupling pattern, which is closely related to the classical VB concept of resonance, combined with the changes in the orbital overlap integrals, show that the reaction path involves a region in which the electronic structure of the reacting system becomes similar to that of benzene. This suggests that during the Claisen rearrangement the reacting system can attain moderately aromatic character but that this does not necessarily happen at the TS. The results of the SC analysis indicate that the most appropriate schematic representation of the Claisen rearrangement is furnished by a homolytic mechanism in which six harpoons describe the changes in the bonding pattern from reactant to product.

Keywords Spin-coupled approach · Claisen rearrangement · Reaction mechanisms · Valence-bond theory

J. G. Hill · P. B. Karadakov (✉)
Department of Chemistry, University of York, Heslington,
York YO10 5DD, UK
E-mail: pbk1@york.ac.uk

D. L. Cooper
Department of Chemistry, University of Liverpool,
Liverpool L69 7ZD, UK

1 Introduction

The rearrangement of allyl vinyl ether is the simplest Claisen rearrangement and therefore, its proper description is an essential prerequisite to understanding the mechanisms of [3,3]-sigmatropic shifts in general. A traditional reaction mechanism, of the type commonly seen in organic chemistry textbooks, takes the form of Scheme A, in which movements of electron pairs are represented by curly arrows and we have added a convenient numbering scheme for the atomic centres. It is obvious that this mechanism shows considerable analogy with the Cope rearrangement of 1,5-hexadiene. Indeed, both rearrangements feature a chair transition state (TS) structure, and are believed to follow concerted pathways [1–4]. The link between the mechanisms of these isoelectronic rearrangements has prompted investigation into the mechanism of an amino-Claisen rearrangement in allyl vinyl amine [5], in which the addition of three methyl substituents to this system produces a reaction that is known to be facile [6].

The scope of the Claisen rearrangement in synthetic chemistry envelopes an overwhelming number of applications. Yet while both experimental [7, 8] and theoretical methods [1, 2, 5, 9–18] have been employed to probe the reaction mechanism, a convincing explanation has yet to be provided. Full and partial substitution of the atoms in the Claisen rearrangement have been studied in detail with both ab initio and density functional methods [9–12]. The combined work of Aviyente, Yoo and Houk [10–12] has demonstrated that careful substitution can decrease the activation barrier to the rearrangement, for example, by placing a cyano derivative at the 2 position [11]. Whilst studies of this type can be of substantial aid to the synthetic chemist, they very much correspond to the limit of what theoretical chemistry can achieve with 'standard' techniques and do not provide a full understanding of the electronic structure rearrangements occurring during the reaction.

Previous theoretical investigations have produced different TS geometries, which range from 1,4-diyl (AM1) [15] to bis-allyl extremes [predicted by CASSCF(6,6)/6-31G*] [1]. The Hartree-Fock (HF) and B3LYP geometries (see Refs. 17

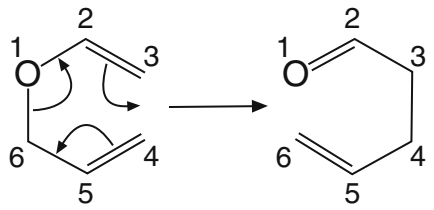

A

and 1, respectively) lie between these two extremes and the MP2 wavefunction produces a structure [17] closer to a 1,4-diyl geometry. Previous verifications of the TS and related predictions of the reaction mechanisms have generally relied upon calculating kinetic isotope effects (KIEs) for various TS geometries. Those values can be compared with the experimentally derived KIEs so as to identify the correct TS. Using this methodology, Wiest, Black and Houk [1] concluded that the B3LYP and BLYP density functionals provide the most reliable TS geometries. These TS geometries suggest an aromatic character, with bond lengths of 2.31–2.43 Å for the forming C−C bond, and 1.90–1.96 Å for the breaking C–O bond. In a subsequent study, Meyer, DelMonte and Singleton [13] corrected the experimental KIE values and also allowed for a tunnelling correction within their theoretical KIE estimates. As a consequence of poor correlations between the theoretical and experimental KIEs, the AM1 and CASSCF TS geometries could be discarded, and the best TS description was found to be the one provided by the MP4(SDQ)/6-31G* wavefunction. This description was closely matched for accuracy by MP2/6-31G* results, which were observed to have a 0.14% RMS error for KIEs compared to 0.13% in the case of MP4(SDQ). This analysis led to the conclusion that the actual TS geometry is most likely in-between the B3LYP/6-31G* and MP2/6-31G* results, implying that the TS has both 1,4-diyl and bis-allyl properties.

Using the nucleus-independent chemical shifts (NICS) [19] methodology to predict aromaticity, Jiao and Schleyer calculated the chemical shift at the mid-point of the forming ring in the parent Claisen rearrangement [14]. The TS geometries utilised were computed at the B3LYP/6-311+G** level of theory, for both boat and chair isomers, and produced HF-GIAO/6-31G* NICS values of −18.5 and −21.2 ppm, respectively. The results of those authors are in good agreement with previous calculations, which predicted the chair-like form to be lower in energy and indicated that the TS is aromatic. For reference, the NICS value for benzene at the same level of theory is −13.4 ppm, which suggests that the chair TS for the Claisen rearrangement is even more aromatic than the ground state of benzene.

In the choice of methods for geometry optimisations, the present study follows closely the work of Meyer et al. [13] by locating the TS and the intrinsic reaction coordinate (IRC) of the Claisen rearrangement with B3LYP/6-31G*, MP2/6-31G* and MP4(SDQ)/6-31G* wavefunctions. The use of different levels of theory enables us to investigate the influence of variations in the geometries at the TS, and along the reaction path, on the electronic mechanism. We study the changes in the electronic structure of the reacting system along the three IRCs by performing spin-coupled (SC) calculations at the TS and at selected IRC geometries. This is followed by analyses of the changes in the shapes of the non-orthogonal SC orbitals, the overlaps between these orbitals, and the active space spin-coupling pattern. An analogous technique was recently employed to probe the competition between aromatic and diradical character in the TS of the parent Cope rearrangement [20], the nature of which was shown to depend directly on the separation between the two fragments in the TS.

2 Computational procedure

In addition to the B3LYP/6-31G*, MP2/6-31G* and MP4(SDQ)/6-31G* geometry optimisations for the TS of the gas-phase Claisen rearrangement of allyl vinyl ether, we also calculated the CCD/6-31G* TS geometry so as to be able to compare with previously reported higher-level computational results. All TS geometries were confirmed as first-order saddle points on the corresponding energy hypersurfaces by diagonalisation of the analytical Hessians, with the exception of the MP4(SDQ) and CCD cases where numerical Hessians were utilised. All TS geometry optimisations met the 'very tight' convergence criteria within GAUSSIAN03 [21], and the MP2, MP4(SDQ) and CCD calculations were performed with all electrons included in the correlation calculation, i.e. without a frozen core. GAUSSIAN03 was also employed to determine the MP2/6-31G*, MP4(SDQ)/6-31G* and B3LYP/6-31G* IRCs, as well as for CASSCF(6,6) and CASMP2 calculations.

SC/6-31G* calculations were then carried out at the B3LYP/6-31G*, MP2/6-31G* and MP4(SDQ)/6-31G* TS geometries, and at points $\pm 1.2\,\mathrm{amu}^{1/2}$bohr away from the TSs, taken from the respective IRCs. We utilised a SC wavefunction involving six 'active' orbitals (ψ_1–ψ_6), all of which are singly occupied and non-orthogonal, and twenty doubly occupied orthogonal 'inactive' or core orbitals (ϕ_1–ϕ_{20}). This SC wavefunction can be written as

$$\Psi_{00}^{6} = \mathrm{A}\left[\left(\prod_{i=1}^{20}\phi_i\alpha\phi_i\beta\right)\left(\prod_{\mu=1}^{6}\psi_\mu\right)\Theta_{00}^{6}\right] \tag{1}$$

where $\hat{\mathrm{A}}$ is the antisymmetriser and Θ_{00}^{6} is the active space spin function (with total spin and its z-component both equal to zero). Θ_{00}^{6} is a general linear combination of all five possible unique spin functions for a singlet system of six electrons.

$$\Theta_{00}^{6} = \sum_{k=1}^{5} C_{0k}\Theta_{00;k}^{6} \tag{2}$$

The active and core orbitals were represented as standard molecular orbital expansions within the 6-31G* basis. All of the corresponding basis function coefficients, and the spin-coupling coefficients defining Θ_{00}^{6}, were determined fully

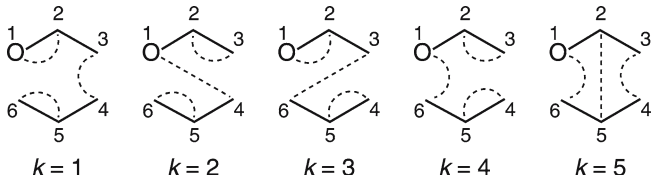

Fig. 1 Rumer spin function ($^{R}\Theta^{6}_{00;k}$) diagrams for the Claisen rearrangement of allyl vinyl ether

variationally, by minimising the energy expectation value corresponding to the SC wavefunction (1) [22–24].

Whilst the SC code used here to carry out the calculations works in the Kotani spin basis [25, 26], it is more convenient to discuss the spin-coupling patterns observed at different stages of the Claisen rearrangement of allyl vinyl ether in terms of the Rumer spin basis [25, 26]. The interconversion between different bases of spin eigenfunctions can be performed easily via SPINS [27], a specialised code for the symbolic generation and transformation of spin eigenfunctions. Each of the five unique Rumer functions for a six electron singlet system is formed as the product of three singlet two-electron spin functions:

$$
\begin{aligned}
^{R}\Theta^{6}_{00;1} &\equiv (1-2, 3-4, 5-6)\\
^{R}\Theta^{6}_{00;2} &\equiv (1-4, 2-3, 5-6)\\
^{R}\Theta^{6}_{00;3} &\equiv (1-2, 3-6, 4-5)\\
^{R}\Theta^{6}_{00;4} &\equiv (1-6, 2-3, 4-5)\\
^{R}\Theta^{6}_{00;5} &\equiv (1-6, 2-5, 3-4)
\end{aligned}
\tag{3}
$$

One convenient complete set of Rumer-style diagrams corresponding to $^{R}\Theta^{6}_{00;1} - ^{R}\Theta^{6}_{00;5}$ for the Claisen rearrangement of allyl vinyl ether is shown in Fig. 1. Couplings 1 and 4 are obvious analogues to the two Kekulé-type structures in benzene, while the three remaining couplings resemble Dewar-type structures. The 1,4-diyl character can be associated with one of the Dewar-like Rumer spin functions within the active space spin-coupling pattern (see Eq. 2), $5 \equiv (1-6, 2-5, 3-4)$, while the remaining two Dewar-like Rumer spin functions, $2 \equiv (1-4, 2-3, 5-6)$ and $3 \equiv (1-2, 3-6, 4-5)$, are responsible for the bis-allyl character.

Spin functions expressed in the Rumer spin basis are usually analysed using one of two weighting schemes, namely either that due to Chirgwin and Coulson [28] or the inverse-overlap scheme of Gallup and Norbeck [29]. Chirgwin–Coulson ($^{R}P^{CC}_{k}$) and Gallup–Norbeck ($^{R}P^{GN}_{k}$) weights are defined, respectively, as:

$$
{}^{R}P^{CC}_{0k} = {}^{R}C_{0k} \sum_{l=1}^{5} (\langle {}^{R}\boldsymbol{\Theta}^{6}_{00} | {}^{R}\boldsymbol{\Theta}^{6}_{00} \rangle)_{kl} {}^{R}C_{0l} \tag{4}
$$

and

$$
\begin{aligned}
{}^{R}P^{GN}_{0k} &= c({}^{R}C_{0k})^{2} / (\langle {}^{R}\boldsymbol{\Theta}^{6}_{00} | {}^{R}\boldsymbol{\Theta}^{6}_{00} \rangle^{-1})_{kk},\\
c^{-1} &= \sum_{k=1}^{5} ({}^{R}C_{0k})^{2} / (\langle {}^{R}\boldsymbol{\Theta}^{6}_{00} | {}^{R}\boldsymbol{\Theta}^{6}_{00} \rangle^{-1})_{kk}
\end{aligned}
\tag{5}
$$

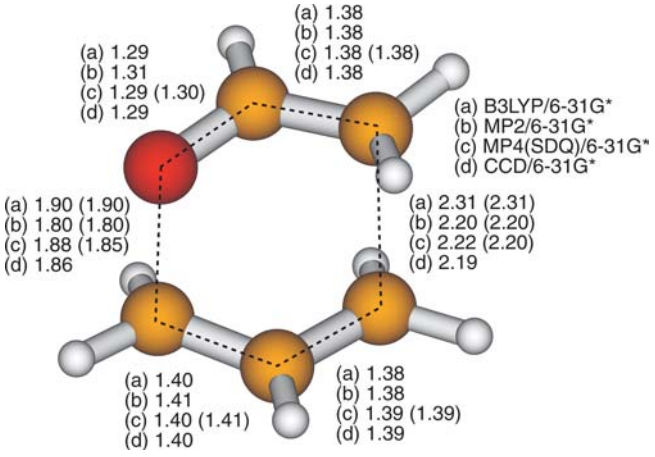

Fig. 2 Optimised transition state geometries of allyl vinyl ether, bond lengths in Å. The B3LYP, MP2 and MP4(SDQ) values in brackets are from Refs. 1, 17 and 13, respectively

where $\langle {}^{R}\boldsymbol{\Theta}^{6}_{00} | {}^{R}\boldsymbol{\Theta}^{6}_{00} \rangle$ denotes the overlap matrix between the spin functions in Eq. 3. Whilst the Gallup–Norbeck weights are restricted to the range 0–1, there is no guarantee that the Chirgwin–Coulson weights will lie within this range, despite the fact that both types of weighting sum up to unity. The advantage of the Chirgwin–Coulson weights lies in the fact that they are linear so that, for example, the total weight of the Kekulé structures in a system is given simply by the sum of the weights of the corresponding Rumer functions.

3 Results and discussion

Selected bond lengths from the optimised B3LYP/6-31G*, MP2/6-31G*, MP4(SDQ)/6-31G* and CCD/6-31G* chair TS geometries for the Claisen rearrangement are presented in Fig. 2, alongside the results of Meyer et al. [13]. The CCD/6-31G* bond lengths are practically equivalent to their MP4(SDQ)/6-31G* counterparts which shows that there would be little point in going beyond the MP4(SDQ) level of theory in the TS and IRC calculations for this reaction. The fact that the MP4(SDQ), CCD and QCISD approaches produce very similar TS geometries suggests a reasonable degree of 'convergence' with respect to the level of theory, at least for post-HF wavefunctions based on the standard closed-shell HF reference.

The separations between the O1–C2–C3 and C4–C5–C6 fragments at the reaction coordinate points corresponding to distances of ± 1.2 amu$^{1/2}$bohr from the TS are shown in Fig. 3. Once again, there are only small differences between the MP4(SDQ)/6-31G* and MP2/6-31G* numbers, and these are also in good agreement with the corresponding values for the geometries from the B3LYP/6-31G* IRC.

The changes occurring in the six SC orbitals during the course of the Claisen rearrangement are illustrated in Fig. 4. Column (b) corresponds to the MP2/6-31G* TS geometry (see Fig. 2), while columns (a) and (c) show orbital snapshots at the IRC $= -1.2$ amu$^{1/2}$bohr and IRC $= +1.2$ amu$^{1/2}$bohr

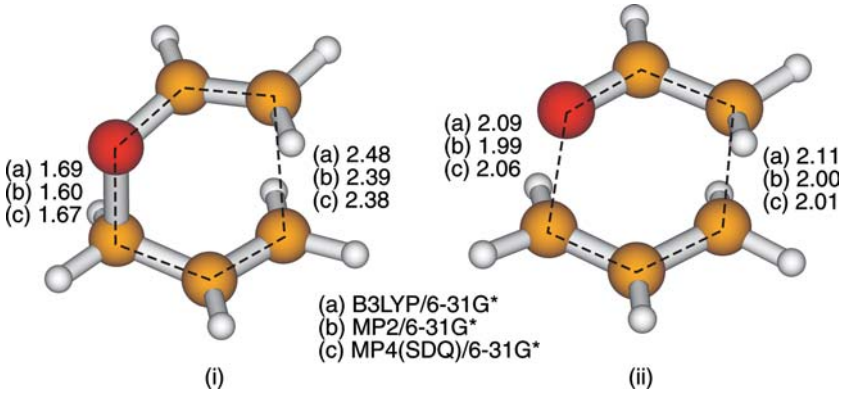

Fig. 3 Reacting system geometries for the Claisen rearrangement of allyl vinyl ether: (i) at IRC $= -1.2\,\mathrm{amu}^{1/2}$bohr from the TS; (ii) at IRC $= +1.2\,\mathrm{amu}^{1/2}$bohr from the TS. Bond lengths in Å

geometries from the MP2/6-31G* IRC (see Fig. 3), i.e. before and after the TS, respectively.

The pictures of the SC orbitals at the B3LYP/6-31G* and MP4(SDQ)/6-31G* TS geometries are not shown separately because they are so similar to their MP2/6-31G* counterparts that it is impossible to distinguish between them by eye.

The SC orbitals at the MP2/6-31G* TS geometry [see column (b) of Fig. 4] are reminiscent of those produced in the SC investigation of the Cope rearrangement [20], with additional distortions caused by the presence of the oxygen atom. Each orbital is localised on a single atom, with the exception of ψ_6 which is partially delocalised onto the strongly electronegative oxygen. Orbitals ψ_2 and ψ_5 are visually similar to those observed in the SC description of benzene [30–32], with the bulges pointing towards adjacent orbitals.

The weights of the Rumer spin functions from the SC calculations at the B3LYP/6-31G*, MP2/6-31G* and MP4(SDQ)/6-31G* TS geometries are displayed in Table 1, in both the Chirgwin–Coulson and Gallup–Norbeck forms. In all three cases the spin-coupling pattern is dominated by the fourth Rumer function, $4 \equiv (1-6, 2-3, 4-5)$. This spin function corresponds to one of the two Kekulé structures and contains the three singlet pairs that are consistent with the three stronger bonding interactions suggested by the shapes of the TS SC orbitals in Fig. 4, ψ_1–ψ_6, ψ_2–ψ_3 and ψ_4–ψ_5. The spin function with the second largest weight at all TS geometries was observed to be $1 \equiv (1-2, 3-4, 5-6)$, which corresponds to the second Kekulé structure. The dominant weights of the two Kekulé-like Rumer spin functions suggest that the system exhibits a certain degree of resonance. However, in the classical valence bond (VB) description of an aromatic system such as benzene, the two Kekulé structures should have equal weights. Clearly this is not observed at any of the three TS geometries for the Claisen rearrangement of allyl vinyl ether that we analysed.

The Chirgwin–Coulson weights of Rumer spin function $5 \equiv (1-6, 2-5, 3-4)$ at the B3LYP/6-31G*, MP2/6-31G* and MP4(SDQ)/6-31G* TS geometries are 0.0861, 0.1220 and 0.1155, respectively (see Table 1). This shows that the 1,4-diyl character is at its lowest in the B3LYP/6-31G* TS geometry, which is not surprising given that this geometry features the largest separation between the O1–C2–C3 and C4–C5–C6 fragments (see Fig. 2). However, the difference between the 1,4-diyl characters of the MP2/6-31G* and MP4(SDQ)/6-31G* structures turns out to be much smaller than would be expected from a consideration only of the distances shown in Fig. 2. According to the data in Table 1, the combined Chirgwin–Coulson weights of Rumer spin functions $2 \equiv (1-4, 2-3, 5-6)$ and $3 \equiv (1-2, 3-6, 4-5)$ at the B3LYP/6-31G*, MP2/6-31G* and MP4(SDQ)/6-31G* TS geometries are 0.1918, 0.1336 and 0.1673, respectively. This confirms the expected decrease of the bis-allyl character on passing from the B3LYP/6-31G* to the MP2/6-31G* structure, as well as the intermediate position of the MP4(SDQ)/6-31G* structure. As can be readily verified, an analysis based on the Gallup–Norbeck weights (see Table 1) leads to much the same qualitative picture.

The overlap integrals $\langle\psi_\mu|\psi_\nu\rangle$ that correspond to the SC orbitals shown in the central column of Fig. 4 are listed in Table 2, for neighbouring orbitals only. In parallel with the distribution of the weights of the Rumer spin functions, the overlaps between corresponding pairs of orbitals for all three TS geometries are decidedly similar. The overlaps between orbitals ψ_2 and ψ_3, and orbitals ψ_4 and ψ_5, have values in the range of 0.61–0.64, which are typical for the SC description of a π bond [33]. It is interesting to note that the overlap of orbitals ψ_1 and ψ_6, corresponding to the breaking carbon–oxygen bond, is still larger than those of the π-bonds that remain in the system, and almost twice as large as that

Table 1 Rumer spin functions in the active space spin-coupling pattern (Θ^6_{00}) for the TS in the Claisen rearrangement at the B3LYP/6-31G*, MP2/6-31G* and MP4(SDQ)/6-31G* geometries, expressed as both Chirgwin–Coulson (P_k^{CC}) and Gallup–Norbeck (P_k^{GN}) weights

		B3LYP		MP2		MP4	
k	Rumer function	P_k^{CC}	P_k^{GN}	P_k^{CC}	P_k^{GN}	P_k^{CC}	P_k^{GN}
1	(1-2, 3-4, 5-6)	0.1556	0.1167	0.1288	0.0852	0.1794	0.1468
2	(1-4, 2-3, 5-6)	0.0720	0.0322	0.0545	0.0187	0.0627	0.0255
3	(1-2, 3-6, 4-5)	0.1198	0.0771	0.0791	0.0362	0.1046	0.0621
4	(1-6, 2-3, 4-5)	0.5665	0.7300	0.6155	0.7841	0.5377	0.6922
5	(1-6, 2-5, 3-4)	0.0861	0.0440	0.1220	0.0758	0.1155	0.0734

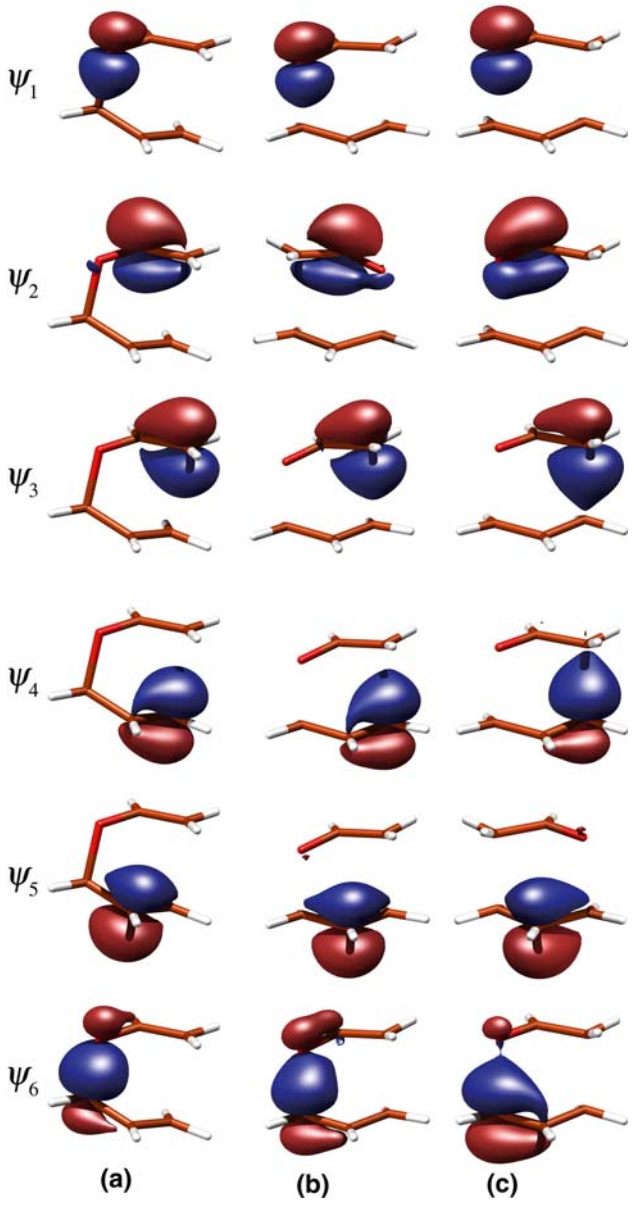

Fig. 4 Spin-coupled orbitals ψ_1-ψ_6 for the Claisen rearrangement along the MP2 IRC: **(a)** IRC $= -1.2\,\text{amu}^{1/2}$bohr, **(b)** IRC $= 0.0\,\text{amu}^{1/2}$bohr (TS), and **(c)** IRC $= +1.2\,\text{amu}^{1/2}$bohr. Three-dimensional isovalue surfaces corresponding to $\psi_\mu = \pm 0.08$ were obtained from Persistence of Vision Raytracer (POV-Ray) files generated by MOLDEN [34]

between ψ_3 and ψ_4, in the forming carbon–carbon bond. For an aromatic system, it is expected that all overlap integrals between adjacent orbitals would in general be very similar in value. As such, the orbital overlaps at all three TS geometries for the Claisen rearrangement provide further evidence of the absence of aromaticity.

An investigation into the TS of a reaction is not sufficient for a complete understanding of the electronic rearrangements that take place on the way from reactants to products. Analyses of the SC calculations at points on either side of the TS along the reaction coordinate are necessary for identifying the nature and extent of the bond breaking and bond formation processes; additionally, one should not discard the possibility that the reacting system may become aromatic in regions somewhat removed from the TS.

Table 2 Overlap integrals between neighbouring orbitals from the SC wavefunctions for the B3LYP/6-31G*, MP2/6-31G* and MP4(SDQ)/6-31G* TS geometries of the Claisen rearrangement

	Overlap					
Geometry	$\langle\psi_1\|\psi_2\rangle$	$\langle\psi_2\|\psi_3\rangle$	$\langle\psi_3\|\psi_4\rangle$	$\langle\psi_4\|\psi_5\rangle$	$\langle\psi_5\|\psi_6\rangle$	$\langle\psi_6\|\psi_1\rangle$
B3LYP/6-31G*	0.4347	0.6404	0.3414	0.6162	0.3073	0.6529
MP2/6-31G*	0.3711	0.6308	0.3561	0.6144	0.3029	0.6856
MP4(SDQ)/6-31G*	0.4351	0.6319	0.3633	0.6066	0.3123	0.6626

In repetition of the observed close similarity between the SC solutions at the B3LYP/6-31G*, MP2/6-31G* and MP4(SDQ)/6-31G* TS geometries, the preliminary SC calculations at each of the corresponding IRC $= \pm 1.2\,\text{amu}^{1/2}$bohr points (see Fig. 3) also furnished almost indistinguishable results. As a consequence, we present and discuss here only the results of SC calculations at the MP2/6-31G* IRC geometries; the SC results at B3LYP/6-31G* and MP4(SDQ)/6-31G* IRC geometries would be very similar indeed.

Let us follow the evolution of shapes of the active orbitals from the SC/6-31G* wavefunction along the MP2/6-31G* reaction path. Well before the TS, at IRC $= -1.2\,\text{amu}^{1/2}$bohr [see column (a) in Fig. 4], orbitals ψ_1 and ψ_6 still form a well-defined C–O σ bond (as in the reactant), slightly distorted towards the oxygen due to its higher electronegativity. The two allyl vinyl ether π bonds can be associated with the ψ_2–ψ_3 and ψ_4–ψ_5 orbital interactions (here and further in the text we refer to bonds that are almost π in nature simply as 'π bonds'). As the reaction proceeds to the TS [see column (b) in Fig. 4], the orbitals remain localised on the atomic centres with which they were associated initially. While it is difficult to discern any change in the O-based orbital ψ_1, it is clear that ψ_2, ψ_5 and ψ_6 'grow tails' at the TS in the directions of ψ_1, ψ_6 and ψ_5, respectively; the opposing lobes of orbitals ψ_3 and ψ_4 become more pointed and come slightly closer. The further evolution of the orbital shapes after the TS leads to a new bonding pattern which is well-established by IRC $= +1.2\,\text{amu}^{1/2}$bohr [see column (c) in Fig. 4]. The appearance of orbital ψ_1 is still much the same as at the TS and at IRC $= -1.2\,\text{amu}^{1/2}$bohr but, due to the re-shaping of orbital ψ_2, it is obvious that ψ_1 and ψ_2 are now engaged in a C–O π bond. The second π bond is realised by orbitals ψ_5 and ψ_6, while the opposing sharper-pointed ψ_3 and ψ_4, which resemble C-based sp^3 hybrids, overlap to form the central C–C σ bond of 1-pentenal. Although the shape of orbital ψ_6 suggests that the C–O σ bond is still not fully broken at IRC $= +1.2\,\text{amu}^{1/2}$bohr, it is clear that at this stage of the reaction orbitals ψ_1 and ψ_6 are both involved to larger degrees in other orbital interactions, with orbitals ψ_2 and ψ_5, respectively.

The variation of the SC orbital overlap integrals $\langle\psi_\mu|\psi_\nu\rangle$ along the reaction path is illustrated in Fig. 5. Once again, as in Table 2, we focus on the overlaps only between adjacent orbitals, because those between non-adjacent orbitals

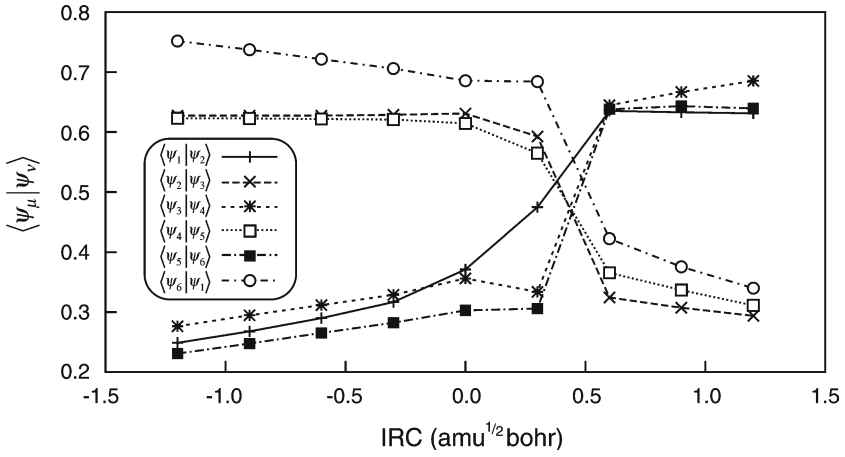

Fig. 5 Variation of the overlap integrals $\langle\psi_\mu|\psi_\nu\rangle$ of SC neighbouring orbitals along the MP2 IRC for the Claisen rearrangement

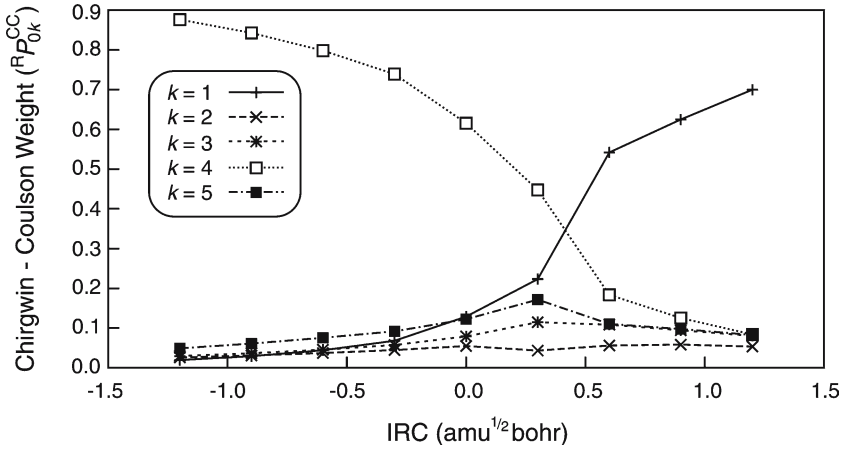

Fig. 6 Composition of the active space spin-coupling pattern for the Claisen rearrangement expressed in the Rumer spin basis along the MP2 IRC

are much smaller in magnitude and do not reveal additional information about the bond breaking and bond formation processes. The curves in Fig. 5 closely parallel the changes observed in the subsequent columns of SC orbitals in Fig. 4. The orbital overlap variations suggest that the reaction follows a concerted mechanism, with bonds breaking and forming almost simultaneously.

The highest overlap on the allyl vinyl ether side of the reaction is $\langle\psi_1|\psi_6\rangle$, between the orbitals involved in the C–O bond. Initially, the allyl vinyl ether π bonds are almost isolated and, correspondingly, the overlaps associated with these bonds are very much the same. The orbital overlaps at the TS suggest that in spite of the fact that the bond breaking and bond formation processes are already underway, the electronic structure of the reacting system is still very similar to that of allyl vinyl ether.

The changes in the active space spin-coupling pattern Θ^6_{00} (see Eq. 2) during the course of the Claisen rearrangement of allyl vinyl ether can be tracked in Fig. 6. At either end of the IRC, the spin-coupling pattern is dominated by a single Kekulé-type spin function, namely $4 \equiv (1-6, 2-3, 4-5)$ (see Eq. 3) at IRC $= -1.2$ amu$^{1/2}$bohr and $1 \equiv (1-2, 3-4, 5-6)$ at IRC $= +1.2$ amu$^{1/2}$bohr. This is the anticipated result, as these Rumer spin functions reflect the bonding patterns in the reactant and products, respectively. All remaining Rumer spin eigenfunctions (corresponding to Dewar-type structures) retain low weights throughout the entire reaction coordinate. The curves for the two Kekulé-type spin functions cross in the same IRC region as the orbital overlap curves corresponding to breaking and forming bonds (see Fig. 5). Away from this crossing region, the active space spin function quickly assumes a form suitable for the reactant or product. All major spin recoupling and orbital overlap changes within the active space occur over a relatively short IRC interval of about 0.5 amu$^{1/2}$bohr. For comparison, the corresponding changes for the Diels-Alder reaction take place over an even shorter IRC interval of just about 0.2 amu$^{1/2}$bohr [33]. Inspection of Fig. 5 suggests that the increase in the length of the IRC interval required for the switch from a reactant-like to a product-like electronic structure can be

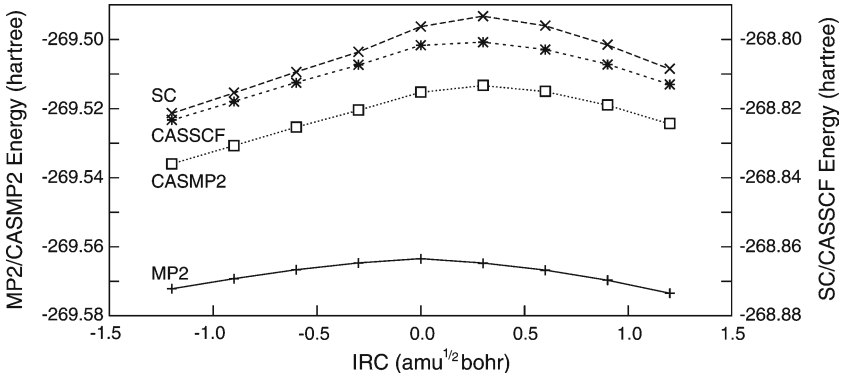

Fig. 7 SC, CASSCF, CASMP2 and MP2 energy profiles along the MP2 IRC

associated mainly with the gradual, non-abrupt formation of the new C–O π bond involving orbitals ψ_1 and ψ_2.

As can be seen in Figs. 5 and 6, the weights of the two Kekulé-type spin functions $1 \equiv (1-2, 3-4, 5-6)$ and $4 \equiv (1-6, 2-3, 4-5)$, become the same at IRC $\approx$ 0.4 amu$^{1/2}$bohr, while all overlaps between neighbouring SC orbitals attain reasonably similar values of ca. 0.45 and ca. 0.55 for C–C and C–O based pairs of orbitals, respectively. At this stage, the electronic structure of the reacting system in the Claisen rearrangement of allyl vinyl ether exhibits features which closely mimic those of its counterpart in the Diels-Alder reaction [33] at a different, earlier part of the corresponding reaction path. In the case of the Diels-Alder reaction, the weights of the two Kekulé-type spin functions were observed to become identical, in parallel with an almost complete equalisation of the overlaps between all neighbouring SC orbitals to ca. 0.51, within a short IRC interval close to the TS. The obvious similarities to essential features in the SC description of the electronic structure of benzene, in combination with a comparison of the respective VB resonance energies, furnished a convincing post-HF level proof that the Diels-Alder reaction passes through an aromatic stage. To claim that the reacting system in the Claisen rearrangement of allyl vinyl ether achieves a comparable degree of aromaticity would be an exaggeration. However, there is sufficient evidence to suggest that after the MP2 TS in the direction of 1-pentenal, within a short segment of the reaction path near IRC $\approx$ 0.4 amu$^{1/2}$bohr, it would be more appropriate to consider the reacting system as moderately aromatic instead of non-aromatic. Given that this reaction path segment is situated past the MP2 TS, it would have been overlooked in an investigation dealing only with the electronic structure of the TS at any of the geometries shown in Fig. 2 which were obtained with methods that would be the first choices of a computational chemist looking at the Claisen rearrangement.

A similar, albeit much smaller separation between the MP2 TS and the centre of the IRC region over which the SC wavefunction switches from a reactant-like to a product-like form was also observed in the very recent SC study of the electronic mechanism of the hetero-Diels-Alder reaction of acrolein and ethene [35].

The fact that, in the case of the Claisen rearrangement, the most pronounced changes in the SC wavefunction are observed after the MP2 TS suggests that the SC energy maximum along the MP2 IRC can also be expected to occur after the MP2 TS. Indeed, the SC energy profile along the MP2 IRC shown in Fig. 3 reaches its maximum at IRC $\approx$ 0.3 amu$^{1/2}$bohr, very close to the crossing points of the curves for the overlap integrals corresponding to breaking and forming bonds in Fig. 5, and for the weights of the two Kekulé-type spin functions in Fig. 6. It is well-known that the SC wavefunction with N active orbitals provides a close, much easier-to-interpet, approximation to the corresponding 'N in N' CASSCF wavefunction. As a consequence, the SC wavefunction, just as its CASSCF counterpart, includes only non-dynamic correlation effects. On the other hand, as was mentioned in the Introduction, the proper ab initio description of the geometry of the TS requires a construction that includes dynamic correlation effects, such as MP2 or MP4(SDQ). This raises the question whether the SC wavefunction, which does not include dynamic correlation effects, would be able to provide a correct account of the changes in the electronic structure of the reacting system along the MP2 IRC. In order to address this issue, we have calculated two additional energy profiles along the MP2 IRC (see Fig. 3). The first of these utilises a '6 in 6' CASSCF wavefunction [CASSCF(6,6)/6-31G*] and, as anticipated, is very close to the SC energy profile. The second energy profile corresponds to a CASMP2 construction which includes both dynamic and non-dynamic effects and is superior to the MP2 approach used to determine the IRC. This energy profile was computed by means of the orthogonal VB MP2 (OVB-MP2) MCSCF perturbation theory method [36] implemented in GAUSSIAN03, on top of the CASSCF(6,6)/6-31G* reference. The importance of the use of second-order perturbation theory treatments based on a CASSCF reference in the description of the potential energy surfaces of pericyclic reactions is well-known (see e.g. Ref. 37), and we would have calculated both the TS geometry and the IRC for the Claisen rearrangement using an approach of this type, if the required codes were available.

The SC, CASSCF and CASMP2 energy profiles in Fig. 3 reach their maxima at very much the same IRC point, IRC $\approx$ 0.3 amu$^{1/2}$bohr. This fact, together with the proximity of the

SC and CASSCF energy profiles, is a reliable indication that the SC wavefunction captures the essence of the electronic structure characteristics carried by the CASSCF reference which dominates the CASMP2 wavefunction. If we had been able to calculate the TS geometry and the IRC using the CASMP2 construction (GAUSSIAN03 does not include CASMP2 gradients), it is very likely that we would have reached the conclusion that the TS for the Claisen rearrangement is moderately aromatic. The extent of the changes in the SC orbital shapes across the three columns of orbitals in Fig. 4 shows that the SC description of the electronic reaction mechanism is not overly sensitive to relatively small variations in the geometries of the reacting system along the IRC. As a result, even if we had been able to calculate a CASMP2 IRC, the subsequent SC analysis would not have produced a qualitatively different picture.

The two most important elements of the electronic structure reorganisation occurring during the Claisen rearrangement of allyl vinyl ether are the changes in the shapes of the six SC orbitals, each of which remains attached to a single atomic centre throughout the reaction (see Fig. 4), and the striking reshuffle in the balance of the weights of the reactant-like and product-like Kekulé-type Rumer spin-coupling schemes (see Fig. 6). Clearly, the active space of the reactant is very much the product of three singlet orbital pairs, ψ_1–ψ_6, ψ_2–ψ_3 and ψ_4–ψ_5, which describe the bonds that are to break during the reaction. None of the reactant orbital pairs is preserved in the product; instead, the six orbitals re-engage in three new singlet orbital pairs, ψ_1–ψ_2, ψ_3–ψ_4 and ψ_5–ψ_6, corresponding to new bonds. This new detailed information about the evolution of the electronic structure of the reacting system during the Claisen rearrangement of allyl vinyl ether strongly suggests that the traditional heterolytic-style representation of the reaction mechanism (see Scheme A in the Introduction), as adopted in many organic chemistry textbooks, is somewhat misleading if used for much more than an electron-counting aid. None of the changes in the active space of the SC wavefunction suggest the movements of three electron pairs implied by the arrows in Scheme A. Instead, our results show that the reaction follows a homolytic mechanism which can be described using six harpoons, as in Scheme B.

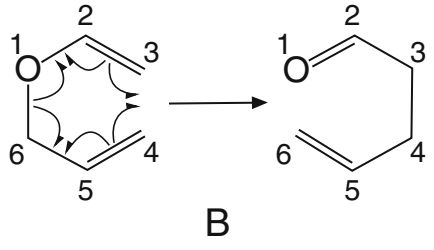

B

4 Concluding remarks

The SC model for the electronic mechanism of the gas-phase Claisen rearrangement of allyl vinyl ether presented in this work indicates that the reaction follows a homolytic mechanism which can be denoted simply using a scheme with six harpoons; these depict the almost simultaneous breaking of the central C–O σ bond and of the two C–C π bonds in allyl vinyl ether, and the formation of two new π bonds (C–O and C–C) and a new C–C σ bond within the product of the reaction, 1-propenal.

The apparent similarity between the SC/6-31G*//B3LYP/6-31G*, SC/6-31G*//MP2/6-31G* and SC/6-31G*//MP4(SDQ)/6-31G* descriptions of the TS, and similarly for the respective IRC $= \pm 1.2\,\mathrm{amu}^{1/2}\mathrm{bohr}$ geometries, suggests strongly that essential qualitative features of the SC description of the reaction mechanism are very unlikely to be influenced by further refinement of the computational methodology used for the TS geometry optimisation and for the calculation of the reaction path. The fact that the MP4(SDQ), CCD and QCISD approaches produce very similar TS geometries lends further support to this statement. Still, the related geometry variations lead to subtle differences between the active space spin-coupling patterns within the SC/6-31G*//B3LYP/6-31G*, SC/6-31G*//MP2/6-31G* and SC/6-31G*//MP4(SDQ)/6-31G* TS wavefunctions which, as we have shown, can be used to quantify the interplay between the 1,4-diyl and bis-allyl character of the corresponding transition structures.

Despite the presence of a highly electronegative oxygen atom, the homolytic mechanism of the Claisen rearrangement in allyl vinyl ether turns out to be very similar to those of the Diels-Alder reaction of butadiene and ethene [33] and of the disrotatory ring-opening of cyclohexadiene [38]. Just as in the cases of these previously studied reactions, here again the homolytic mechanism allows the reacting system to attain some degree of aromatic character. However, in the present case, the 'mid-point' in the bond breaking and bond formation processes, in the neighbourhood of which the reacting system exhibits aromatic features, is shifted to well after the geometric MP2 TS along the reaction path in the direction of the 1-propenal product. The extent of this shift appears to be dependent on the method used to optimise the TS and calculate the reaction path, and while the shift will be much the same if these calculations utilise post-HF approaches based on a closed-shell HF reference, or DFT, it is likely to become very small or even disappear if the calculations could be carried out using a second-order perturbation theory treatment based on a CASSCF reference.

References

1. Wiest O, Black KA, Houk KN (1994) J Am Chem Soc 116:10336
2. Vance RL, Rondan NG, Houk KN, Jensen F, Borden WT, Komornicki A, Wimmer E (1988) J Am Chem Soc 110:2314
3. Hrovat DA, Morokuma K, Borden WT (1994) J Am Chem Soc 116:1072
4. Oliva JM (1999) Theor Chem Acc 103:1
5. Yamabe S, Okumoto S, Hayashi T (1996) J Org Chem 61:6281
6. Hill RK, Gilman NW (1967) Tetrahedron Lett 1421
7. Schuler FW, Murphy GW (1950) J Am Chem Soc 72:3155
8. Gajewski JJ, Brichford NL (1994) J Am Chem Soc 116:3165

9. Burrows CJ, Carpenter BK (1981) J Am Chem Soc 103:6984
10. Yoo HY, Houk KN (1997) J Am Chem Soc 119:2877
11. Aviyente V, Young HY, Houk KN (1997) J Org Chem 62:6121
12. Aviyente V, Houk KN (2001) J Phys Chem A 105:383
13. Meyer MP, DelMonte AJ, Singleton DA (1999) J Am Chem Soc 121:10865
14. Jiao H, Schleyer PvR (1998) J Phys Org Chem 11:655
15. Dewar MJS, Jie C (1989) J Am Chem Soc 111:511
16. Yoo HY, Houk KN (1994) J Am Chem Soc 116:12047
17. Davidson MM, Hillier IH, Vincent MA (1995) Chem Phys Lett 246:536
18. Hu H, Kobrak MN, Xu C, Hammes-Schiffer S (2000) J Phys Chem A 104:8058
19. Schleyer PvR, Maerker C, Dransfield A, Jiao H, Hommes NJvE (1996) J Am Chem Soc 118:6317
20. Blavins JJ, Cooper DL, Karadakov PB (2004) J Phys Chem A 108:194
21. Frisch MJ, Trucks GW, Schlegel HB, Scuseria GE, Robb MA, Cheeseman JR, Montgomery JA, Vreven T, Kudin KN, Burant JC, Millam JM, Iyengar SS, Tomasi J, Barone V, Mennucci B, Cossi M, Scalmani G, Rega N, Petersson GA, Nakatsuji H, Hada M, Ehara M, Toyota K, Fukuda R, Hasegawa J, Ishida M, Nakajima T, Honda Y, Kitao O, Nakai H, Klene M, Li X, Knox JE, Hratchian HP, Cross JB, Adamo C, Jaramillo J, Gomperts R, Stratmann RE, Yazyev O, Austin AJ, Cammi R, Pomelli C, Ochterski JW, Ayala PY, Morokuma K, Voth GA, Salvador P, Dannenberg JJ, Zakrzewski VG, Dapprich S, Daniels AD, Strain MC, Farkas O, Malick DK, Rabuck. AD, Raghavachari K, Foresman JB, Ortiz JV, Cui Q, Baboul AG, Clifford S, Cioslowski J, Stefanov BB, Liu G, Liashenko A, Piskorz P, Komaromi I, Martin RL, Fox DJ, Keith T, Al-Laham MA, Peng CY, Nanayakkara A, Challacombe M, Gill PMW, Johnson B, Chen W, Wong MW, Gonzalez C, Pople JA (2003) Gaussian 03, Revision B.03. Gaussian Inc, Pittsburg
22. Karadakov PB, Gerratt J, Cooper DL, Raimondi M (1992) J Chem Phys 97:7637
23. Gerratt J, Cooper DL, Karadakov PB, Raimondi M (1997) Chem Soc Rev 97:87
24. Gerratt J, Cooper DL, Karadakov PB, Raimondi M (2003) In: Wilson S (ed) Handbook of molecular physics and quantum chemistry, vol 2, chap 12. Wiley, New York
25. Pauncz R (1979), Spin eigenfunctions. Plenum Press, New York
26. Karadakov PB (2003) In: Wilson S (ed) Handbook of molecular physics and quantum chemistry, vol 2, chap 3. Wiley, New York
27. Karadakov PB, Gerratt J, Cooper DL, Raimondi M (1995) Theor Chim Acta 90:51
28. Chirgwin BH, Coulson CA (1950) Proc Roy Soc Lond Ser A 201:196
29. Gallup GA, Norbeck JM (1973) Chem Phys Lett 21:495
30. Cooper DL, Gerratt J, Raimondi M (1986) Nature 323:699
31. Gerratt J, Chem Br 23:327 (1987)
32. Cooper DL, Wright SC, Gerratt J, Hyams PA, Raimondi M (1989) J Chem Soc Perkin Trans 2:719
33. Karadakov PB, Cooper DL, Gerratt J (1998) J Am Chem Soc 120:3975
34. Schaftenaar G, MOLDEN (A Pre- and Post Processing Program of Molecular and Electronic Structure). CAOS/CAMM Centre, University of Nijmegen, The Netherlands
35. Blavins JJ, Cooper DL, Karadakov PB (2005) J Phys Chem A 109:231
36. McDouall JJW, Peasley K, Robb MA (1988) Chem Phys Lett 148:183
37. Borden WT, Davidson ER (1996) Acc Chem Res 29:67
38. Karadakov PB, Cooper DL, Thorsteinsson T, Gerratt J (2000) In: Hernández-Laguna A, Maruani J, McWeeny R, Wilson S (eds) Quantum systems in chemistry and physics, vol 1. Basic problems and model systems. Kluwer, Dordrecht, pp 327–344